

Electron spectroscopy of nanocrystalline diamond surfaces

J. ZEMEK*, J. HOUDKOVA, B. LESIAK^a, A. JABLONSKI^a, J. POTMESIL, M. VANECEK
Institute of Physics, Academy of Sciences of the Czech Republic, 162 53 Praha 6, Czech Republic
^a*Institute of Physical Chemistry, Polish Academy of Sciences, ul. Kasprzaka 44/52, 01-224 Warszawa, Poland*

Thin, fully optically transparent nanocrystalline diamond (NCD) films prepared at growth temperatures from 400 °C to 1100 °C were characterized by scanning electron microscopy (SEM), atomic force microscopy (AFM), angular-resolved x-ray photoelectron spectroscopy (ARXPS) and elastic peak electron spectroscopy (EPES). The ARXPS spectra were applied for estimating the extent of sp³ hybridization of carbon atoms in a surface region of the NCD films. Processing of the ARXPS C 1s lines indicated that above 90 % of carbon atoms exhibiting the sp³ hybridization in the analyzed volume. The very top surface was found to be less enriched with the sp³ hybridized carbon atoms. The inelastic mean free paths (IMFP) of electrons in NCD films were evaluated in the electron energy range 200 eV – 2400 eV from the measurement of the electron elastic backscattering probability and the Monte Carlo (MC) calculations of electron transport. The resulting IMFPs were compared to the IMFPs calculated from the optical data and from the TPP-2M predictive formulae, where pronounced difference between both sources of calculated IMFP values was found. The EPES IMFPs in five NCD films indicated no differences. Close agreement of the present IMFPs to those calculated from the optical data was found.

(Received October 11, 2006; accepted November 2, 2006)

Keywords: Nanocrystalline diamond film, Electron microscopy, X-ray photoelectron spectroscopy, Electronic structure, Surface properties

1. Introduction

The nanocrystalline diamond (NCD) films have recently attracted considerable interest due to possible important technological applications [1]. Such films can be used for various tribological coatings and as hard, wear resistant biocompatible materials [2] exhibiting a low friction coefficient. A major advantage in comparison to polycrystalline diamond films is, in particular, their relative low surface roughness. However, similarly to microcrystalline diamond, the grain boundary properties, the grain size and consequently sp²/sp³ concentration in the NCD films can be significantly altered. Presently, the NCD film technology becomes a trivial task. Generally, there are two basic ways how to prepare the NCD films, either using argon-based gas chemistry [3-6] or hydrogen-based gas chemistry [7,8]. All other modifications (adding of N₂ or increasing CH₄) have been also successfully tested [7]. However, there is still a lack of knowledge about the film quality grow at low temperature range (below 600 °C). It is well known that films grown from Ar-based chemistry are “black” due to sp² carbon atoms in a matrix. Now, we have succeeded to grow the NCD films at or even below 400 °C. This opens a new field for numerous applications where temperature sensitive substrates are used. Important question remains: are these films also of such a good quality as those grown at high substrate temperature, 700 °C – 900 °C?

The NCD films are usually deposited from the methane/hydrogen/argon plasma onto substrates with a high nucleation density value of 10¹⁰-10¹¹ cm⁻² [9-12]. The

NCD films under study are undoped, fully optically transparent below 5.4 eV, photosensitive, with Raman signature of predominant diamond bonding. Nevertheless, diamond grains of nanometric dimensions (about 50 – 100 nm) would be surrounded by differently bonded carbon atoms, e.g. by the sp² hybridized carbons [13]. Therefore, in addition to the sp³ bonded carbon atoms, also some percentage of the sp² hybridized carbon atoms is expected, especially at the sample surface. To elucidate the nanostructure in a vicinity of the diamond nanograins at the film surfaces, we applied a surface-sensitive method that is able to characterize a site-specific chemical environment.

The angular-resolved X-ray induced photoelectron spectroscopy (ARXPS) is usually applied to the C 1s photoelectron line for differentiating two contributions originated from the sp² and the sp³ hybridized carbon atoms. Curve fitting of the C 1s spectrum relies upon a theoretical basis [14,15]. Predicted chemical shift, about 1 eV, is mostly due to different relaxation energy associated with different electronic configuration of the carbon atom [16]. The Elastic peak electron spectroscopy (EPES) is the experimental method widely applied for determining the electron transport parameters in a solid, i.e. the inelastic mean free path (IMFP) values of electrons and their kinetic energy dependence [17]. The IMFPs are especially important in quantitative electron spectroscopy methods, i.e. XPS, Auger electron spectroscopy (AES, XAES), etc., for determining the surface composition, the overlayer thickness, the non-destructive depth profiling of elements found near solid surfaces, and for calculations of electron

transport in a solid. The EPES method combines the measurement of the electron elastic backscattering probability from an investigated sample and a standard material (so-called method with a standard) with the relevant Monte Carlo (MC) calculations of the electron transport in a solid. The methods for evaluating the IMFPs for selected elements, inorganic and organic compounds in the electron energy range 50 eV – 10 000 eV have been extensively reviewed [17]. These IMFPs are available in the NIST database [18]. Recently, the IMFPs for diamond and graphite have been calculated from the optical data by Tanuma et al. [19]. The relevant IMFP values can be also calculated from the TPP-2M predictive formulae [20]. Surprisingly large root-mean-square (RMS) deviations were found between the IMFPs calculated from TPP-2M and those evaluated from the optical data for diamond (71.8%) and graphite (49.5%) [19]. At present, the number of reliable experimental IMFP data obtained with the EPES spectroscopy for diamond [17] is very limited. Up to the best present authors knowledge, the first attempt to determine the IMFPs for a NCD film has been done very recently by the EPES method using a Cu standard [21]. Note, a single crystal or polycrystalline diamond sample surface with large grains are less convenient for assessment of the IMFPs than the NCD samples since no coherent effects are expected in the recorded spectra. Their occurrence makes calculations of electron transport difficult.

In the present work, NCD films deposited at growth temperatures from 400 °C to 1100 °C are investigated using the XPS and the EPES spectroscopy methods. The results focus on characterizing the content of sp^3 hybridized carbon atoms in the analyzed volume using the analysis of the C 1s XPS line, as well as on determining the IMFPs by the EPES method for five NCD film surfaces in the electron energy range 200 eV – 2400 eV and their comparison to theory.

2. Experimental

2.1. Samples

The NCD films were deposited from the methane/hydrogen microwave plasma on (100) oriented, 15x15 mm² silicon substrates [22]. Prior to deposition process, all substrates were pretreated under identical conditions [9,10] applying a modified “bias enhanced nucleation” (BEN) process in a microwave plasma enhanced chemical vapor deposition system (Aixtron P6). The substrates were biased with DC power supply. After a first substrate-cleaning step (12 min in hydrogen plasma), the BEN process was applied for 8 min (-180 V at the substrate, 5% of methane in hydrogen, 20 mbar, and 850 °C). A nucleation density reached 10^{10} - 10^{11} cm⁻². During the growth step, methane concentration was held constant at 1% CH₄ in H₂ and the substrate temperature, controlled via substrate holder stage, varied between 400 °C and 1100 °C. Temperatures below 600 °C were measured by the two-color pyrometer working at the

wavelengths of 2.13 mm and 2.35 mm (Williamson type) and temperatures above 600 °C were measured by the two-color pyrometer working at the wavelengths of 1.35 mm and 1.55 mm (CHINO type). Both pyrometers were found to be insensitive to the quartz bell jar. This procedure enabled a growth of the NCD films at growth temperatures of 400 °C, 500 °C, 890 °C and 1100 °C. Their thickness extracted from the transmission interferometry measurements [23, 24] ranged from 100 to 1200 nm. Optical transparency of thicker films was checked in the spectral range from 200 nm to 25 μm using Hitachi UV-IR spectrometer by light transmission through the self-supporting NCD membrane prepared by silicon substrate etching [12].

The standard sample for the EPES analysis was prepared in a form of a gold film by “ex-situ” vacuum evaporation of Au on the Si(111) substrate.

2.2. Electron spectroscopy methods

The NCD films were transported into the electron spectrometer through air without “ex-situ” and “in-situ” surface cleaning. Particularly, ion beam cleaning has led to essential structural changes in the treated diamond surface [25]. The surface composition and bonding of the NCD layers were studied by XPS using an ADES-400 angular-resolved photoelectron spectrometer (VG Scientific, U.K.) equipped with a twin anode X-ray source (the standard Al/Mg anodes) and a hemispherical analyzer. The half-cone acceptance angle of the analyzer was set to 4.1°. The XPS spectra were recorded using Mg K_α source operated at a power of 200 W at constant pass energy of 100 eV or 20 eV, at emission angles with respect to the surface normal equal to 0° and 60°.

The EPES spectra were measured in ADES-400 spectrometer from NCD films and Ar⁺ beam (energy of 4000 eV, current density 1×10^{-5} Acm⁻²) sputter cleaned Au film surface. The electron source beam current varied from 0.1 μA to 1.0 μA with the beam spot diameter at the sample surface of ~ 3 mm. The electron backscattering intensities (elastic peak areas) were recorded in the primary electron kinetic energy range from 200 eV to 2400 eV. The geometry of the EPES analysis was the following: (i) the primary beam normal to the sample surface, (ii) the electron emission angle 35° with respect to the surface normal and (iii) the half-cone acceptance angle of the analyzer 4.1°. The typical half-width (FWHM) of the elastic peak spectra recorded in the applied energy range was ~ 0.5 eV.

3. Results and discussion

3.1. Surface characterization

Before proceeding with the XPS quantification of the NCD films, the energy scale of the spectrometer has been calibrated with respect to the Au 4f_{7/2} line maximum at 84.0 eV. The NCD film surfaces cleanliness was evaluated

from the XPS C 1s and O 1s peak areas, determined following the Shirley's inelastic background subtraction and normalized for the measured transmission function of the spectrometer, which comprises all instrumental factors influencing the measured quantity [26], the photoelectric cross-sections [27], and for the relevant inelastic mean free paths of photoelectrons [19]. These normalized values represent the average composition within the analyzed volume [28]. At the pristine NCD film surfaces 2-3 at. % of oxygen was found (Table 1).

Table 1. Comparison of parameters characterizing preparation conditions: thickness, oxygen content, and carbon atoms bonding at the NCD film surfaces. Notation: T_s – substrate temperature during the NCD film growth. FWHM – C 1s full width at half maximum.

Sample	T_s (°C)	thickness (nm)	emission angle (°)	O (at %)	C 1s fitting FWHM	C sp^3 (%)
1	400	130	0	2.6	1.1	96.8
			60	-	1.2	92.9
2	500	106	0	2.3	1.0	98.5
			60	-	1.2	94.7
3	890	1230	0	2.5	1.0	95.3
			60	-	1.2	95.2
4	890	490	0	2.3	1.0	96.3
			60	-	1.1	93.9
5	1100	470	0	2.1	1.0	96.9
			60	-	1.1	92.7

Fig 1 shows a typical SEM image of one of the thickest NCD film (i.e. one with the largest grains) grown at 800 °C. The average grain size is 100 nm for a film thickness of 900 nm. We have observed that NCD films with thickness up to 1000 nm can be still classified as nanocrystalline with average grain size not exceeding 100 nm. When the film thickness is larger than this particular value, the average grain size increases and the film becomes polycrystalline. The thinner films grown at 400 °C – 500 °C reveal smaller grains in the order of 10 nm – 20 nm.

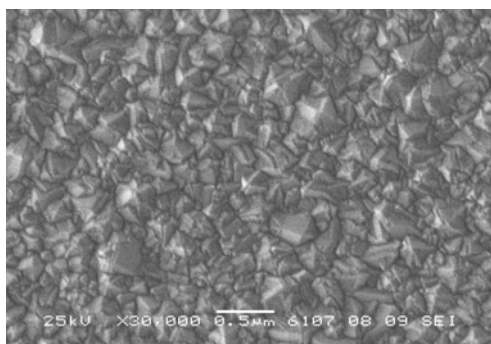


Fig. 1. Typical SEM image of the pristine NCD film 900 nm thick grown on Si(100) at 800 °C.

The *RMS* value of the surface roughness, estimated by AFM, ranged from 10 nm to 30 nm depending on the NCD film thickness. More details about the film preparation and basic characterization (Raman, SEM, optical transmittance) can be found elsewhere [12].

The percentage of the sp^3 hybridized carbon atoms in the analyzed volume of the NCD films was evaluated from the high resolution C 1s XPS spectra recorded at two emission angles, i.e. 0° and 60° with respect to the surface normal. These C 1s spectra are relatively narrow (about 1.1 eV) and slightly asymmetric indicating several C bonding states involved. The C 1s spectra were processed after subtracting a Shirley background by the non-linear least-square method fitting procedure. Three functions (mixed 5% Lorentzian – 95% Gaussian) located at 284.2 eV, 285.1 eV, and 286.1 eV were fitted to the measured C 1s spectral line shapes. The first binding energy position can be easily ascribed to the sp^2 contribution and it agrees well with that for graphite [29]. The last binding energy position can be ascribed to C-O bonding, in agreement with the handbook data [29]. The middle binding energy value that dominates in the intensity for all the NCD film surfaces would be ascribed to the sp^3 contribution (the diamond phase). The latter is shifted to the higher binding energy from the sp^2 contribution due to the more effective core hole screening in carbon atoms in trigonal coordination [16]. Since the diamond is a wide gap material and the C 1s line is referred to the Fermi level, the binding energy value of the sp^3 contribution depends on a doping and on a state of the surface. For this reason, the measured binding energy of diamond scatters considerably [14,30-32]. In the present analysis, we rely on the theoretical support predicting the chemical shift of ~1 eV. Haerle et al. [14] calculated the C 1s shift between the sp^2 and sp^3 contributions to the C 1s peak in amorphous carbon systems by molecular dynamics simulations. The shift was found to be about 1.0 eV. The recent first-principles calculations of the C 1s core-level shift between the C sp^2 and C sp^3 contributions for a series of amorphous carbon density revealed almost the same value 1.1 ± 0.2 eV [15]. The calculations agree well with the measured and fitted C 1s lines [14,31,32]. These calculations provide strong support for decomposing the XPS spectra into two peaks resulting from sp^2 and sp^3 hybridized carbon atoms [16]. The exemplary high-resolution C 1s spectra recorded from the NCD film grown at 500 °C, measured at emission angles of 0° and 60°, and the results of the non-linear fitting procedure are shown in Figs 2 (a) – (b), respectively. Comparison of the resulting percentage of sp^3 hybridized carbon atoms, calculated from C 1s (sp^2) and C 1s (sp^3) peaks for the NCD films, and the parameters of the applied fitting procedure are listed in Table 1. The resulting percentage of sp^3 hybridized carbon atoms for all grown NCD films is above 90 %. Generally, this percentage is larger below the surface region (from 95.3 % to 98.5 %) than at the surface region (from 92.7 % to 95.2 %). No remarkable differences in the sp^3 percentage among the five NCD

films prepared in the temperature range $400^{\circ}\text{C} - 1100^{\circ}\text{C}$ were observed (Table 1), which indicates an excellent quality of the film grown also at the lower temperature.

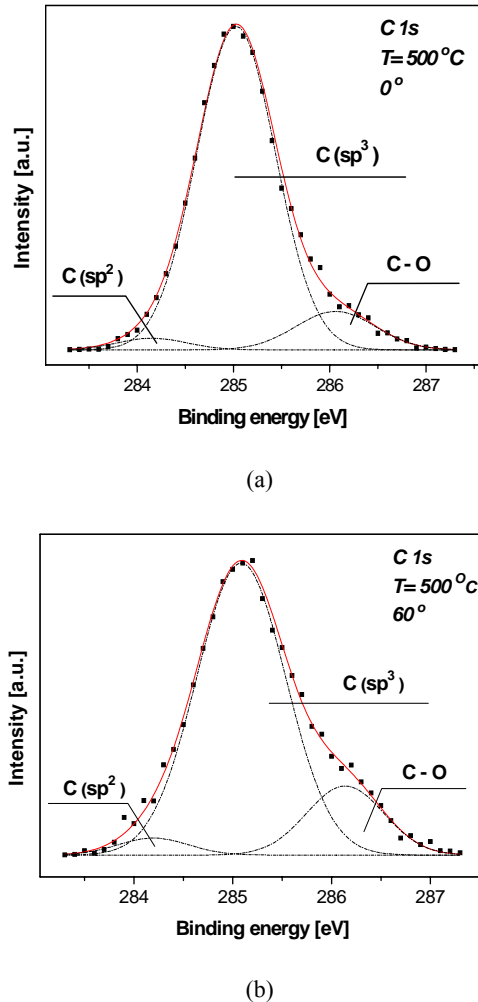


Fig. 2. The exemplary high-resolution C 1s spectra of the NCD film grown at 500°C with 98.5 % and 94.7 % of sp^3 hybridized carbon atoms in the analyzed volume as measured at two emission angles with respect to the surface normal. (a) 0° , (b) 60° , respectively.

The difference in the measurement geometry of C 1s photoelectron transition leads to variation of the mean photoelectron probing depths. Specifically, the mean probing depth, given as a product of the IMFP and cosine of the emission angle [33], resulted in 1.6 nm and 0.8 nm for emission angles of 0° and 60° , respectively. The observed differences evaluated from two geometries of the measurement of the C 1s line (Figs 2 (a) – (b), Table 1) are consistent and indicate the surface slightly contaminated with oxygen, as well as slightly enriched with carbon atoms in trigonal configuration. Similar observations have recently been published by Birrell et al. [13].

3.2. Inelastic mean free path

The MC algorithm of electron transport in a solid was described in details elsewhere [34,35]. The model assumes smooth surface, uniform atomic composition and density, the elastic scattering events along the trajectory length following the Poisson stochastic distribution with the distribution of distances between elastic collisions as a function of the electron elastic mean free path and the polar scattering angles with respect to the initial direction described by the probability density function dependent on the total elastic mean free path and the electron differential elastic scattering cross-sections. An important step in the MC calculations, using the software EPESWIN [35], is selecting the electron elastic scattering cross-sections, described in details elsewhere [36,37], based on potential describing interactions between an electron and the scattering atom. Present calculations involve the potential derived from the relativistic Hartree-Fock self-consistent method, i.e. the Dirac-Hartree-Fock (DHF) potential.

The EPES measurements and the MC calculations were carried out for the same geometry of measurement and electron kinetic energies. In the MC calculations, the recommended IMFP was selected for the Au standard [17], whereas for the investigated sample, the calculations proceeded assuming a set of the IMFPs ranging from 0.1 to 30 nm. From the calculated dependences of the electron elastic backscattering ratio as a function of the IMFP, called the calibration curves, and the respective EPES measured ratio, the IMFP values for the sample are evaluated. The kinetic energy dependence of the electron IMFPs obtained with the EPES method and Au standard averaged over the five NCD films is shown in Fig. 3.

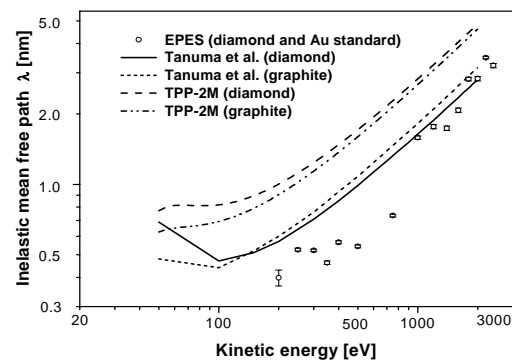


Fig. 3. Comparison of IMFP values and their energy dependence in the NCD films, diamond and graphite. Circle: the EPES IMFPs obtained with the Au standard averaged over the five NCD films. Solid line: diamond - Tanuma et al. [19]. Short-dashed line: graphite - Tanuma et al. [19]. Long-dashed line: diamond - TPP-2M [20] predictive formula. Double-dotted dashed line: graphite - TPP-2M [20] predictive formula.

These are compared to the IMFPs calculated by Tanuma et al. and the IMFPs resulting from the TPP-2M predictive formula IMFPs for diamond and graphite

[19,20]. The *RMS* and the percentage (*R*) deviations were evaluated according to Eqn (1)

$$RMS = \left[\left(\frac{1}{r} \sum_{j=1}^r (\lambda_{av} - \lambda_i)^2 \right)^{\frac{1}{2}} \right]$$

$$R = 100 \left(\frac{1}{r} \sum_{j=1}^r \left| \frac{\lambda_{av} - \lambda_i}{\lambda_{av}} \right| \right) \quad (1)$$

where λ_{av} are the IMFPs averaged for five NCD films, λ_i are the IMFPs for the five NCD films, $i = 1, 2, \dots, 5$ refers to the NCD film notation (Table 1), and j is the number of electron kinetic energies. The deviations calculated from Eqn (1) are enclosed in Table 2.

The deviations between the IMFPs observed for the five NCD films are of the order of few percent (Table 2) indicating no remarkable differences between the evaluated IMFPs for five NCD films exhibiting different percentage of sp^3 carbon hybridization. Large discrepancies between Tanuma et al. optical IMFPs and the TPP-2M predictive formula IMFPs for graphite and diamond are observed. The EPES IMFPs for NCD are closer to Tanuma et al. optical values, with better approximation to the relevant values for diamond. Better agreement is observed for the electron kinetic energy region 1000 eV – 2400 eV. In the electron energy range from 200 eV to 750 eV, the EPES IMFPs in diamond are smaller than the optical IMFPs by Tanuma et al. [19]. Similar dependence has been observed in the previous work [21].

Table 2. Comparison of scatter (Eqn (1)) between the EPES IMFPs obtained as an averaged value and the EPES IMFPs for respective five NCD films.

Sample	<i>RMS</i> (nm)	<i>R</i> (%)
1	0.065	2.72
2	0.076	4.12
3	0.033	1.70
4	0.121	4.65
5	0.066	2.06

The IMFPs calculated from the optical data are valid for the bulk of the solid, while the IMFPs obtained from the EPES method are influenced by the electron energy losses in the surface region of the solid [38-40]. The electron entering the analyzer, after travelling a given trajectory length in a solid, passes through the surface region twice, which increases the probability of an energy loss, as compared with a trajectory of the same length travelled in the bulk of the solid. Although, the surface

excitation effects are partially cancelled when we use relative measurements (with the standard) [36], they can affect the resulting IMFPs in the low electron energy region [41]. As published previously [21], accounting for the surface excitations slightly increases the EPES evaluated IMFPs. However, the relative differences between the EPES and Tanuma et al. evaluated IMFPs as well as the electron energy dependence remains similar.

4. Summary and conclusions

Nanocrystalline diamond films deposited from the methane/hydrogen plasma were successfully grown at low substrate temperature (400 °C) as well at high temperature (>800 °C). The C 1s lines recorded at two different emission angles and therefore at two different information depths were used to estimate the extent of sp^3 hybridized carbon atoms at the analyzed surfaces. Results indicate that (i) NCD surfaces are dominantly composed from the sp^3 hybridized carbon atoms with a slight enrichment of the top surface by the sp^2 hybridized carbon atoms, (ii) surface quality of all samples was found to be the same irrespective of the growth temperature. The latter property is extremely technologically important for numerous applications necessitating low temperature treatments. Assessment of IMFP values for NCD films by measurements of the electron elastic backscattering probability combined with the Monte Carlo calculations of electron transport facilitated testing two procedures used to calculate the IMFP in diamond. Results showed better agreement of the present IMFP data to those calculated from the optical data.

Acknowledgements

This work was supported by the Institutional Research Plan No. AV0Z10100521, the Czech Science Foundation - projects 202/05/2233 and 202/06/0459. One of the authors (A. J.) would like to acknowledge partial support by the Foundation for Polish Science.

References

- [1] J. Ristein, Appl. Phys. A-Mater. Sci. Process. **82**, 377 (2006).
- [2] L. Tang, W.W. Gerbirich, L. Kruckeberg, D.R. Kanai, Biomaterials **16**, 483 (1995).
- [3] D.M. Gruen, S. Liu, A.R. Krauss, X. Pan, J. Appl. Phys. **75**, 1758 (1994).
- [4] D. M. Gruen, S. Liu, A. R. Krauss, J. Luo, X. Pan, Appl. Phys. Lett. **64**, 1502 (1994).
- [5] D.M. Zhou, T.G. McCauley, L.C. Qin, A.R. Krauss, D.M. Gruen, J. Appl. Phys. **83**, 540 (1998).
- [6] D. M. Gruen, Annu. Rev. Mater. Sci. **29**, 211 (1999).
- [7] K. Subramanian, W. P. Kang, J. L. Davidson, W. H. Hofmeister, Diamond Relat. Mater. **14**, 404 (2005).

- [8] L. Sekaric, J.M. Parpia, H.G. Craighead, *Appl. Phys. Lett.* **81**, 4455 (2002).
- [9] J. Philip, P. Hess, T. Feygelson, J.E. Butler, S. Chattopadhyay, K.H. Chen, L.C. Chen, *J. Appl. Phys.* **93**, 2164 (2003).
- [10] Y. Liu, C. Liu, Y. Chen, Y. Tzeng, P. Tso, I. Lin, *Diamond Relat. Mater.* **13**, 671 (2004).
- [11] V. Mortet, Z. Hubicka, V. Vorlicek, K. Jurek, J. Rosa, M. Vanecek, *Phys. Stat. Sol. (a)* **201**, 2425 (2004).
- [12] V. Mortet, J. D'Haen, J. Potmesil, R. Kravets, I. Drbohlav, V. Vorlicek, J. Rosa, M. Vanecek, *Diamond Relat. Mater.* **14**, 393 (2005).
- [13] J. Birrell, J.A. Carlisle, O. Auciello, D.M. Gruen, J.M. Gibson, *Appl. Phys. Lett.* **81**, 2235 (2002).
- [14] R. Haerle, E. Riedo, A. Pasquarello, A. Baldereschi, *Phys. Rev. B* **65**, 045101 (2002).
- [15] J.T. Titantah, D. Lamoen, *Carbon* **43**, 1311 (2005).
- [16] L. Calliari, *Diamond Relat. Mater.* **14**, 1232 (2005).
- [17] C. J. Powell, A. Jablonski, *J. Phys. Chem. Ref. Data* **28**, 19 (1999).
- [18] C. J. Powell, A. Jablonski. NIST Electron Inelastic Mean Free Path Database, NIST, SRD71, v.1.1, Gaithersburg 2000.
- [19] S. Tanuma, C.J. Powell, D.R. Penn, *Surf. Interface Anal.* **37**, 1 (2005).
- [20] S. Tanuma, C.J. Powell, D.R. Penn, *Surf. Interface Anal.* **21**, 165 (1994).
- [21] J. Zemek, J. Potmesil, M. Vanecek, B. Lesiak, A. Jablonski, *Appl. Phys. Lett.* **87**, 262114 (2005).
- [22] M. Funer, C. Wild, P. Koidl, *Appl. Phys. Lett.* **72**, 1149 (1998).
- [23] R. Swanepoel, *J. Phys. E-Sci. Instr.* **17**, 896 (1984).
- [24] A. Poruba, A. Fejfar, Z. Remes, J. Springer, M. Vanecek, J. Kocka, J. Meier, P. Torres, A. Shah, *J. Appl. Phys.* **88**, 148 (2000).
- [25] P. Reinke, G. Francz, P. Oelhafen, J. Ullmann, *Phys. Rev. B* **54**, 7067 (1996).
- [26] P. Jiricek, *Czech. J. Phys.* **44**, 261 (1994).
- [27] I.M. Band, L.Y. Kharitonov, M.B. Trzhaskovskaya, *Atomic Data Nucl. Data Tables* **23**, 443 (1979).
- [28] C.S. Fadley, R.J. Baird, W. Sickhaus, T. Novakov, S.A. Bergstrom, *J. Electron Spectrosc. Relat. Phenom.* **4**, 93 (1974).
- [29] J.F. Moulder, W.F. Stickle, P.E. Sobol, K.D. Bomben. *Handbook of X-ray Photoelectron Spectroscopy*. Perkin-Elmer Co.: Eden Prairie, MN, 1992.
- [30] J. Diaz, J.A. Martin-Gago, S. Ferrer, F. Comin, L. Abello, G. Loucazeau, *Diamond Relat. Mater.* **1**, 824 (1992).
- [31] L.Yu. Ostrovskaya, A.P. Dementiev, I.I. Kulakova, V.G. Ralchenko, *Diamond Relat. Phenom.* **14**, 486 (2005).
- [32] S. Ferro, M. Dal Cole, A. De Battisti, *Carbon* **43**, 1191 (2005).
- [33] J. Zemek, S. Hucek, A. Jablonski, I.S. Tilinin, *J. Electron Spectrosc. Relat. Phenom.* **76**, 443 (1995).
- [34] A. Jablonski, P. Jiricek, *Surf. Sci.* **412/413**, 42 (1998).
- [35] A. Jablonski, *Surf. Interface Anal.* **37**, 1035 (2005).
- [36] A. Jablonski, F. Salvat, C.J. Powell, *J. Phys. Chem. Ref. Data* **33**, 409 (2004).
- [37] A. Jablonski, F. Salvat, C.J. Powell. NIST ElectronElastic-Scattering Cross-Section Database, Version 3.1, (SRD 64), U. S. Department of Commerce, National Institute of Standards and Technology, Gaithersburg, Maryland, 2003.
- [38] Y.F. Chen, *Surf. Sci.* **380**, 199 (1997).
- [39] W.S.M. Werner, W. Smekal, C. Tomastik, H. Stori, *Surf. Sci.* **486**, L461 (2001).
- [40] Y.F. Chen, *Surf. Sci.* **519**, 115 (2002).
- [41] J. Zemek, P. Jiricek, B. Lesiak, A. Jablonski, *Surf. Sci.* **562**, 92 (2004).

*Corresponding author: zemek@fzu.cz